# Direct Reactive and Active Power Regulation of DFIG using an Intelligent Modified Sliding-Mode Control Approach

Habib Benbouhenni[1*], Hamza Gasmi[2], and Nicu Bizon[3,4,5]

[1]Faculty of Engineering and Architecture, Department of Electrical & Electronics Engineering, Nisantasi University, 34481742 Istanbul, Turkey

[2]Laboratoire Controle Avancé (LABCAV), Department of Electronics and Telecommunications, Université 8 Mai 1945 Guelma BP 401, Guelma 24000, Algeria

[3]Faculty of Electronics, Communication and Computers, University of Pitesti, 110040 Pitesti, Romania

[4]Doctoral School, Polytechnic University of Bucharest, 313 Splaiul Independentei, 060042 Bucharest, Romania

[5]ICSI Energy Department, National Research and Development Institute for Cryogenic and Isotopic Technologies, 240050 Ramnicu Valcea, Romania;

(habib.benbouenni@nisantasi.edu.tr, gasmi.hamza@univ-guelma.dz, nico.bizon@ubit.ro)

[‡]Corresponding Author; Habib Benbouhenni, BP: 50B Ouled Fares Chlef Algeria, Tel: +213663956329,

habib.benbouenni@nisantasi.edu.tr

*Received: 15.12.2022 Accepted:31.12.2022*

**Abstract-** This work presents a novel direct reactive and active power control (DRAPC) of grid-connected doubly-fed induction generator (DFIG)-based dual-rotor wind power systems. The designed DRAPC technique employs an intelligent modified sliding mode controller (IMSMC) to directly calculate the required rotor control voltage so as to eliminate the power ripples and the instantaneous errors of reactive and active powers without involving any synchronous coordinate transformations. Thus, no extra current control loops are required, thereby simplifying the system design and enhancing the transient performance. The rotor inverter is controlled by traditional pulse width modulation, which eases the designs of the power converter and the AC harmonic filter. Simulation results on a 1.5-MW grid-connected DFIG system are provided and compared with those of the traditional DRAPC with proportional-integral controllers. The designed DRAPC technique provides enhanced transient performance similar to the traditional DRAPC technique and minimizes the current, active power, and torque ripples.

**Keywords:** Direct reactive and active power control, intelligent modified sliding-mode controller, doubly-fed induction generator, pulse width modulation, dual-rotor wind power system.

**Nomenclature**

| | |
|---|---|
| DFIG | Doubly-fed induction generator |
| MSMC | Modified sliding mode control |
| WT | Wind turbine |
| DRAPC | Direct reactive and active power control |
| SMC | Sliding mode controller |
| DTC | Direct torque control |
| IMSMC | Intelligent modified sliding mode control |
| PI | Proportional integral |
| DRWT | Dual-rotor wind turbine |
| MSVM | Modified space vector modulation |
| FOC | Field-oriented control |
| PWM | Pulse width modulation |
| THD | Total harmonic distortion |
| AG | Asynchronous generator |
| FL | Fuzzy logic |

## 1. Introduction

Electric energy is among the energies that have been in great demand in recent decades, as a result of its massive invasion of human life, and has become a priority for the

governments of countries as a result of the pressures exerted on it by environmental protection associations from pollution. Electric energy comes from several sources, including renewable sources such as wind and non-renewable sources such as gas. As it is known, the consumption of gas and oil to generate electric power has been declining continuously as a result of the high percentages of $CO_2$ in the atmosphere and climate change, as the ratios of dependence on fossil fuels in 1973 were about to 86%, and in 2016 the percentages of consumption of this fossil fuel were about 81% [1]. The phenomenon of global warming has led the governments of countries to search for other sources and inexpensive solutions to produce electric power and dispense with the use of fossil fuels [2]. Several solutions have been proposed to generate power at the lowest cost and reduce global warming. These solutions are represented in the proposal of power generation systems powered by wind [3], solar energy [4], the potential energy of water [5], and sea waves [6]. Among these sources that are popular and widely spread across the world is wind energy [7], where wind energy participates in a large part of electric power generation around the world and this is done using wind energy through a wind turbine (WT) system that consists of three main components, including wind turbines, gear, and an electric generator [8]. WT systems or what is known as wind stations (wind farms) to generate electric power. These systems convert wind energy into electricity using WTs [9]. The latter are types, and each type has its characteristics and advantages that distinguished it from the rest. WTs can be divided into two main parts, horizontal WTs [10, 11] and vertical WTs [12], where horizontal WTs are the most widespread across the world [13]. In recent years, horizontal WTs have witnessed rapid growth and great development in the size of the WTs rotor, and the emergence of other new types of WTs that are more efficient and durable [14]. Multi-rotor wind turbines (MRWT) are a new technology that has recently emerged as one of the solutions to increase energy production and depends on the use of several turbines to produce energy [15]. In addition, WT system electrical is a complex system and is based on meteorological conditions such as wind speed and other factors [16]. Besides turbines, there is an element or component that is of great importance in the process of generating electric power, which is the electric generator, where the electric generator is the beating heart of the WT system and the element responsible for generating electric current.

In the field of the WT systems, several electric generators are used to generate power such as asynchronous generators (AG) [17], synchronous generators [18], doubly-fed induction generators (DFIGs) [19], and DC generators [20]. To transmit and integrate electrical energy or current into the grid we need power electronics, these power electronics are used to stabilize the frequency at a value of 50 Hz. Therefore, the control system is necessary to transmit and transfer wind power to the electric grid.

In the field of control, there are several strategies suggested controlling electrical machines, especially electric generators such as DFIG. Among these strategies, the following are mentioned: direct torque control (DTC) [21], backstepping command [22], synergetic command [23], sliding mode command (SMC) [24], direct reactive and active power command (DRAPC) [25], vector control [26], passivity control [27], intelligent control [28], and field-oriented control [29]. These control schemes differ in principle and concept, as they can be divided into linear controls and nonlinear controls. DARPC strategy is among the control schemes that have attracted great interest among researchers because of its simplicity, durability, ease of implementation and application compared to several controls such as vector control and FOC strategies [30]. This strategy is a type of linear controls, with the same idea as the DTC strategy [31]. The DRAPC technique depends on the use of a hysteresis comparator to command the active and reactive power and the use of a switching table to generate control signals in IGBT [32]. This control was used to control both the AG [33], DFIG [34], and synchronous generator [35].

Despite the many advantages of the DRAPC technique, there are disadvantages such as active power fluctuations and low current quality [36]. As it is known, low current quality affects electrical devices such as motors and makes operations unstable. Moreover, low current quality increases the periodic maintenance and thus increases the industrial cost and this is undesirable.

To improve the advantages and increase the efficiency of the DRAPC technique of the DFIG-WT system, several new techniques were used, for example, neural networks [37], fuzzy control [38], genetic algorithm [39], backstepping control [40], synergetic control [41].

Traditionally, SMC is one of the controls that appeared in the last century, specifically in the seventies, by the scientist Utkin as a solution to increase durability and improve the dynamic response of systems [42]. This kind of control is characterized by high durability compared to traditional controls, as its use leads to a significant improvement in the efficiency of the systems [43]. In the SMC, there are 2 sections, discontinuous and continuous parts, where the continuous part is related to the system under study [44], which makes it difficult to apply the SMC technique in complex systems such as 7-phase motors. The SMC technique has been used in several different fields such as renewable energies [45-49]. The SMC is characterized by the phenomenon of chattering, which is determined by the use of the SMC technique [50]. In [51], the author uses the SMC to improve the robustness of the DPC technique of the DFIG-WT system. SMC and neural algorithms are combined to control/regulate the active power of the DFIG-WT system [52]. A simplified SMC is proposed to improve the quality of the energy of the MRWT [53]. The simplified SMC technique is a new control technique that is robust, easy to perform, and highly durable. Compared to the traditional SMC technique, the simplified SMC technique is easy to implement in complex systems such as 7-phase motors. An integral SMC technique was used to command the reactive power and improve the characteristic of the AG-based WT [54]. In [55], an improved SMC technique based on fuzzy logic (FL) is presented and confirmed using Matlab software, where the Sing(u) function was replaced by the FL strategy. The combination of FL and SMC improved dynamic response, reduced active power, and current ripples, reduced total

harmonic distortion (THD) of current, and increased system durability. Also, the phenomenon of chattering was remarkably overcome.

In this work, the proposed simplified SMC technique in [53] was combined with fuzzy logic to improve the advantages of the DFIG-controlled DRAPC. The reactive and active forces are regulated using ISSMC controllers, where pulse width modulation (PWM) is used to generate IGBT signals. In addition, the obtained results are compared with the PI controller and it is shown that the dynamic response can be improved and the reactive power ripples reduced by the proposed technique. Moreover, the grid voltage is checked and the THD value of the outgoing current from the DFIG rotor inverter is checked which may cause disturbance in the grid. Simulations in different cases to run and extensive analyzes are presented to show the high performance of the designed strategy.

## 2. MRWT System

Fig. 1 represents the electrical energy generation system used in this work. This system consists of the main components a turbine, DFIG, and a pair of the converter. This system operates in a variable wind speed condition. In addition, an MRWT turbine was used to increase the power gained from the wind and reduce the stresses found in conventional turbines [56]. DFIG was chosen because of its many advantages over several generators, simplicity of control, low cost, durability, and low maintenance are mentioned among these advantages [57].

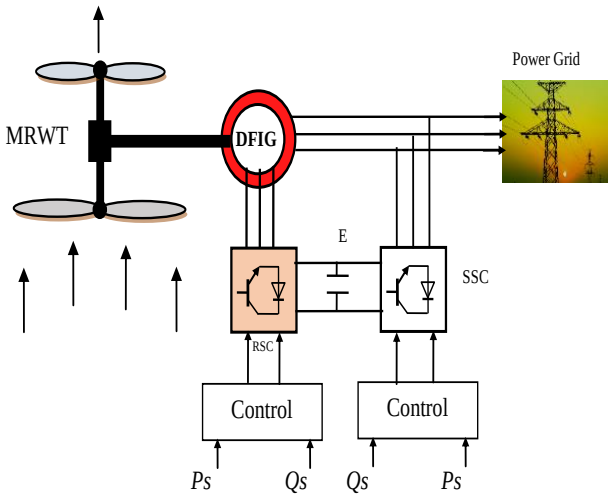


**Fig. 1.** The MRWT system.

### *2.1 MRWT Characteristics*

MRWT is among the new technologies that have appeared recently and have shown great effectiveness in improving the characteristic of the energy generation system compared to the old technology. MRWT is two turbines placed on the same axis to raise the mechanical energy gained from the wind, as this system has been studied in several research works. The mechanical power gained from wind in this technology is 23% times greater than in the old technology. Moreover, it is more robust against winds generated by other wind turbines in wind farms. The downside of this turbine is that it is characterized by complex command compared to the old technology.

The mechanical energy gained from the MRWT is the sum of the two-energy gained from each turbine, which can be expressed by equation (1). On the other hand, the same applies to torque, the value of torque can be given by equation (2). The energy gained from the MRWT is used to rotate the DFIG to generate electric current.

$$T = T_1 + T_2 \tag{1}$$

$$E = E_1 + E_2 \tag{2}$$

where, $E$ and $T$ are the output energy and torque.

Equation (3) represents the torque produced by each turbine [56, 57].

$$\begin{cases} T_1 = \dfrac{1}{2\lambda_1^3}.\rho.\pi.R_1^5.C_p.V_1^2 \\ T_2 = \dfrac{1}{2\lambda_2^3}.\rho.\pi.R_2^5.C_p.V_2^2 \end{cases} \tag{3}$$

where, $\rho$ is the air density, $\lambda_1$ and $\lambda_2$ are the tip speed ration of the first and second turbines, $R_2$ and $R_1$ are the blade radius of the second and first turbines, and $w_2$ and $w_1$ are the mechanical speed of the second and first turbines.

To calculate the torque, we need to know the value of the λ of each turbines and to find out the value of the λ we use equation (4) [53].

$$\begin{cases} \lambda_1 = \dfrac{w_1.R_1}{V_1} \\ \lambda_2 = \dfrac{w_2.R_2}{V_2} \end{cases} \tag{4}$$

where, $V_1$ and $V_2$ are the speed of the unified wind on first and second turbines.

The wind speed of the first turbine is the same as the wind speed. But the wind speed of the second turbine is different from the wind speed before the first turbine, as this speed is related to the distance between the two turbines ($x$) and a constant coefficient ($C_T$) of 0.9. Equation (5) represents the wind speed at any point between the first and second turbines, where the distance between the first and second turbines is 15 meters [53, 57].

$$V_2 = V_1\left(1 - \frac{1-\sqrt{(1-C_T)}}{2}\left(1 + \frac{2.x}{\sqrt{1+4.x^2}}\right)\right) \tag{5}$$

where, $C_T$ is the trust coefficient.

The energy produced by the MRWT system is related to a coefficient called the coefficient of power ($Cp$), where the largest value of this coefficient is 0.59. This coefficient is related to the generator speed, pitch angle ($\beta$), wind speed and can be expressed by equation (6) [56].

$$C_p(\lambda,\beta) = \frac{1}{\lambda + 0.08\beta} - \frac{0.035}{\beta^3 + 1} \tag{6}$$

*2.2 Mathematical Model of DFIG*

In the field of renewable energies, especially WT, DFIG is considered one of the best and most widely used solutions in power generation [58]. The Park transformation is used to give the mathematical form of the DFIG. The DFIG has two parts represented in the electrical part shown in equations (7) through (11) and the mechanical part represented in equations (12) and (13) [59].

The equations (7) and (8) represent the stator and rotor fluxes, respectively.

$$\begin{cases} \psi_{ds} = L_s I_{ds} + M I_{dr} \\ \psi_{qs} = L_s I_{qs} + M I_{qr} \end{cases} \tag{7}$$

$$\begin{cases} \psi_{dr} = L_r I_{dr} + M I_{dr} \\ \psi_{qr} = L_r I_{qr} + M I_{qr} \end{cases} \tag{8}$$

where, $M$ is the mutual inductance, $L_r$ and $L_s$ is the inductance of the rotor and stator, $I_{dr}$ and $I_{qr}$ are the rotor currents, $\Psi_{dr}$ and $\Psi_{qr}$ are the rotor fluxes, $\Psi_{qs}$ and $\Psi_{ds}$ are the stator fluxes.

The rotor voltage and the generator stator voltage are represented in equations (9) and (10), respectively.

$$\begin{cases} V_{dr} = R_r I_{dr} + \dfrac{d}{dt}\psi_{dr} - \omega_r \psi_{qr} \\ V_{qr} = R_r I_{qr} + \dfrac{d}{dt}\psi_{qr} + \omega_r \psi_{dr} \end{cases} \tag{9}$$

$$\begin{cases} V_{ds} = R_s I_{ds} + \dfrac{d}{dt}\psi_{ds} - \omega_s \psi_{qs} \\ V_{qs} = R_s I_{qs} + \dfrac{d}{dt}\psi_{qs} + \omega_s \psi_{ds} \end{cases} \tag{10}$$

Electrical power is of two types, active (*Ps*) and reactive (*Qs*) power. These two powers can be expressed by equation (11).

$$\begin{cases} P_s = \dfrac{3}{2}(V_{ds} I_{ds} + V_{qs} I_{qs}) \\ Q_s = \dfrac{3}{2}(V_{qs} I_{ds} - V_{ds} I_{qs}) \end{cases} \tag{11}$$

The mechanical part of the generator is the relationship between torque and speed. This part can be expressed by equation (12), where the evolution of velocity in terms of torque can be known through this equation [59].

$$T_e - T_r = J \cdot \frac{d\Omega}{dt} + f \cdot \Omega \tag{12}$$

where, $T_r$ is the load torque, $J$ is the inertia, $\Omega$ is the mechanical rotor speed, $T_e$ is the torque, and $f$ is the viscous friction coefficient.

The value of the torque is directly affected by the current, as there is a direct relationship between them and the torque can be expressed by equation (13) [58].

$$T_e = \frac{3}{2} p \frac{M}{L_r} (I_{dr} \cdot \psi_{qs} - I_{qr} \cdot \psi_{ds}) \tag{13}$$

where, $p$ is the number of pole pairs.

## 3. Traditional DRAPC Technique

DRAPC is the command of active and reactive power using both a switching table and two hysteresis controllers, the principle of which is to generate pulses that are applied directly to the inverter switches to generate currents of variable frequency depending on the reference speed [34, 41]. To do this, the active and reactive power must remain within the specified hysteresis ranges to avoid large active power ripples. In this control, we do not need to know the speed of rotation of the generator and the lack of coupling of the *Ps* and *Qs* [53]. A switching table is used to generate the seven non-zero voltage vectors and the zero vector. These eight voltage vector sequences are used to control the inverters, which are energized according to the states of the hysteresis comparators and the position of the voltage vectors [25].

The working principle of this strategy lies in organizing the coefficients of *Ps* and *Qs* and the presence of high-accuracy direct measurements of these parameters by estimating the *Ps* and *Qs* and making a comparison with references to the *Ps* and *Qs*.

In terms of the idea, it is very similar to the DTC, and the difference between them lies in the references used only [35, 36]. Compared to FOC, DRAPC is simple, easy to perform, inexpensive, and characterized by dynamic speed. Fig. 2 represents the DRAPC technique for DFIG. The disadvantages of this technique are that there are ripples at the level of both reactive and active power [53, 36]. Also, the presence of ripples in the network current, minimizes the quality of the current and this is undesirable. Moreover, in this technique, both the reactive and active power must be estimated, which requires the use of high-precision devices

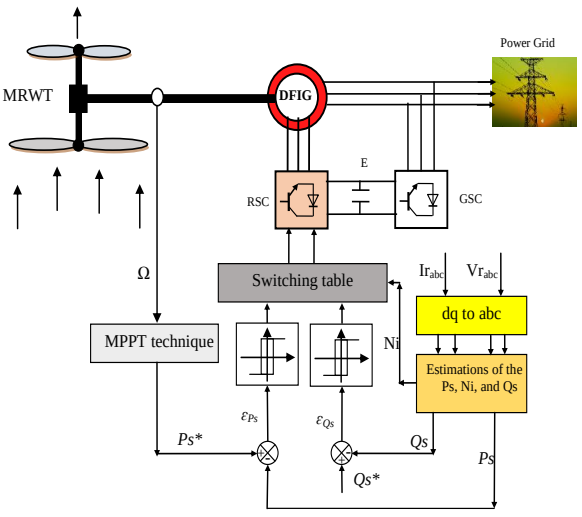


**Fig. 2.** DRAPC technique of the DFIG-based MRWT system

In the DRAPC technique, high-precision measuring devices should be used to measure voltage and current, as these two values are used to estimate the rotor/stator flux. The rotor/stator flux estimation is used to calculate the measured values of both *Ps* and *Qs* of the DFIG. Equation (14) represents the flow estimate corresponding to DFIG [53].

$$\begin{cases} \Psi_{r\alpha} = \int_0^t (v_{r\alpha} - R_r i_{r\alpha})dt \\ \Psi_{r\beta} = \int_0^t (v_{r\beta} - R_r i_{r\beta})dt \end{cases} \quad (14)$$

where, $V_{r\alpha}$ and $V_{r\beta}$ is the rotor voltage linkage of α-β axis.

The rotor flux amplitude is given by:

$$\Psi_r = \sqrt{\Psi_{r\alpha}^2 + \Psi_{r\beta}^2} \quad (15)$$

The rotor flux angle is calculated by :

$$\theta_r = arctg(\frac{\Psi_{r\beta}}{\Psi_{r\alpha}}) \quad (16)$$

Using equation (14) the *Ps* and *Qs* can be expressed by equations (17) and (18), where these two equations are used in order to calculate the error in the *Ps* and *Qs* [41, 53].

$$P_S = -\frac{3}{2}\frac{Lm \times (Vs.\Psi_{r\beta})}{\sigma \times Ls \times Lr} \quad (17)$$

$$Q_S = -\frac{3}{2}(-\frac{Vs.Lm}{\sigma.Ls.Lr} \cdot \Psi_{r\alpha} + \frac{Vs}{\sigma.Ls} \cdot \Psi_{r\beta}) \quad (18)$$

where, $L_m$ is the mutual inductance.

The power estimation can be expressed using both stator/rotor flux. Also, the rotor and stator flux angles are calculated for use in estimating the powers. The equations (19) and (20) represent the estimation of the active and reactive power, respectively.

$$P_s = -\frac{3}{2}\frac{L_m}{\sigma.Ls.Lr} w_s |\psi_s||\psi_r| \sin(\lambda) \quad (19)$$

$$Q_s = -\frac{3}{2}\frac{w_s}{\sigma.Ls}|\psi_s|(\frac{M}{L_r}|\psi_r|\cos(\lambda) - |\psi_s|) \quad (20)$$

With:

$$\sigma = 1 - \frac{M^2}{L_r L_s} \quad (21)$$

Equation (22) is used to calculate the stator flux likage α-axis.

$$\Psi_{s\alpha} = \sigma L_r I_{r\alpha} + \frac{M}{L_s}\Psi_s \quad (22)$$

where, $\Psi_s$ is the stator flux, $\Psi_{s\alpha}$ is the stator flux linkage of α-axis, $I_{r\alpha}$ is the rotor current linkage of α-axis.

Equation (23) is used to calculate the stator flux likage β-axis.

$$\Psi_{s\beta} = \sigma L_r I_{r\beta} \quad (23)$$

where, $I_{r\beta}$ is the rotor current linkage of β-axis, $\Psi_{s\beta}$ is the stator flux linkage of β-axis.

The relationship between voltage and flux can be expressed by equation (24).

$$|\overline{\Psi_s}| = \frac{|\overline{V_s}|}{w_s} \quad (24)$$

where, $V_s$ is the stator voltage.

The reactive and active powers can be reformulated by inducing angle $\lambda$ between the stator and rotor vectors as follows :

$$\frac{dP_s}{dt} = -\frac{3}{2}\frac{L_m}{\sigma.Ls.Lr} w_s |\psi_s| \frac{d(|\psi_r| \sin(\lambda))}{dt} \quad (25)$$

$$\frac{dQ_s}{dt} = -\frac{3}{2}\frac{M.w_s}{\sigma.L_r L_s}|\psi_s|(\frac{d(|\psi_r|\cos(\lambda))}{dt}) \quad (26)$$

In the classical strategy, two hysteresis comparators (HCs) are used to command both the *Ps* and *Qs*, with a 2-level hysteresis comparator for reactive power (see Fig. 3). Besides, a 3-level hysteresis controller for active power is used (see Fig. 4 ).

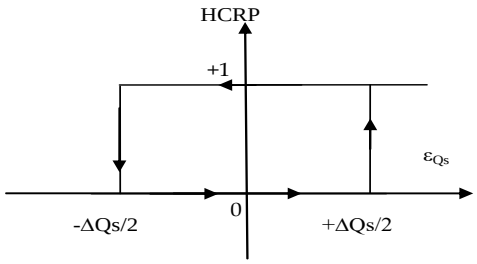


**Fig. 3.** *Qs* hysteresis comparator.

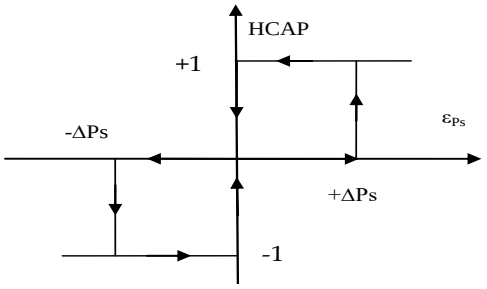


**Fig. 4.** *Ps* hysteresis comparator.

In addition to the use of HCs, a switching table is used to control the generator inverter. This table has three entries: zones, *Ps*-error and *Qs*-error. The outputs are represented by the control signals in the relays of the inverter. Table 1 represents the traditional switching table of the DRAPC strategy [35].

**Table 1.** Switching table for traditional DRAPC

| N | | 1 | 2 | 3 | 4 | 5 | 6 |
|---|---|---|---|---|---|---|---|
| **Hq** | **Hp** | | | | | | |
| **1** | **1** | 5 | 6 | 1 | 2 | 3 | 4 |
| | **0** | 7 | 0 | 7 | 0 | 7 | 0 |
| | **-1** | 3 | 4 | 5 | 6 | 1 | 2 |
| **0** | **1** | 6 | 1 | 2 | 3 | 4 | 5 |
| | **0** | 0 | 7 | 0 | 7 | 0 | 7 |
| | **-1** | 2 | 3 | 4 | 5 | 6 | 1 |

## 4. Proposed IMSMC Technique

Nonlinear techniques are one of the most famous techniques that are characterized by their robustness against changes in system parameters and external factors, and excellent results are estimated in various tests. The SMC technique is among the nonlinear techniques that have been widely spread in several fields because of its advantages, especially in the case of external factors [46, 47]. The negative of this control is the presence of the phenomenon of chattering that determines its uses [45, 49]. In addition, the complexity, especially in cases of complex systems, where is difficult to implement. In [53], the author presented a new idea for this technique under the name modified SMC technique. This strategy is characterized by robustness, ease of implementation and simplicity compared to the traditional SMC technique [53]. Also, it can be easily applied to complex systems.

### *4.1 Design of the MSMC Controller*

MSMC technique is a new technique proposed in order to replace the classical technique and overcome its defects. It was first introduced in [53] to overcome the ripples of the *Ps* and *Qs* of the DFIG. Also, the advantages and disadvantages of the DPC technique are improved. Among the advantages of this method is that it is easy to adjust and has a high dynamic speed. Equation (27) represents the MSMC technique [53].

$$w(t) = K_1.sat(e(t)) + K_2.e(t) \quad (27)$$

where, $K_1$ and $K_2$ are the positive constants ($K_2 \neq 0$).

The response of the MSMC controller can be adjusted using both $K_1$ and $K_2$, where both the genetic algorithm and PSO algorithm can be used to calculate these parameters. Fig. 4 shows the MSMC controller architecture in [53].

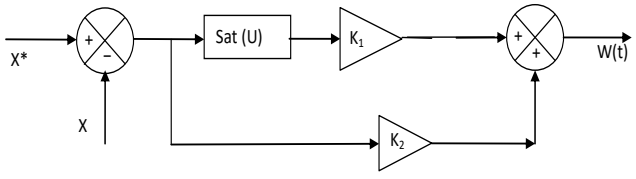


**Fig. 5.** The MSMC controller

To study the stability of the MSMC, Lyapunov theory is used. The latter is often used as a proof of the stability of the roads and depends on the equation (28).

$$\dot{S} \times S \prec 0 \quad (28)$$

The Lyapunov technique makes it possible to pronounce as to the stability of a state equilibrium without resorting to solving the equation of state of the system. Supposing that the equilibrium state is 0.

The sign of a function V(x), (V(0) = 0, V(∞) = ∞), called Lyapunov function, and that of its time derivative $\dot{V}(x) = \frac{dV(x)}{dt}$ give information on the stability of the system. V(x) plays the role of an "energy" function active for the considered system. If $v(x) \succ 0, \forall x \neq 0$ and $\dot{V}(x) \prec 0$ the system is asymptotically stable. A class of classical Lyapunov functions for determining the condition of attractiveness is that of quadratic functions of the type.

$$V(x) = \frac{S^2}{2} \quad (29)$$

In order for the slip variable S (x, t) to tend to zero, the condition shown in equation (30) must be satisfied.

$$\dot{V}(x) = \dot{S} \times S \prec 0 \quad (30)$$

The condition mentioned in equation (30) is not sufficient to guarantee the convergence of the finite time to the surface. To ensure that S (x, t) converges towards 0 at a specific time, a new condition is used which is to use the nonlinear gravitational state represented in equation (31), where this state is called the η attractive state in general.

$$\dot{S} \times S \leq -\eta \times |S|, \eta \succ 0 \quad (31)$$

For *S* is not zero, the following can be written [53]:

$$\dot{S} \leq -\eta \times Sat(e), \eta \succ 0 \quad (32)$$

where, e is the error.

If $S(x) \succ 0, S(x) \leq S(0) - \eta \times t$ and if $S(0) \succ 0, S(t) \geq S(0) + \eta \times t$ So, in all cases, S(x, t) reaches 0 in less than $\frac{|S(0)|}{\eta}$.

This condition is always satisfied in the case of a control of the type represented in equation (33).

$$w(t) = K_1.sat(e(t)) \quad (33)$$

where, η is the positive gain ($\eta = K_1$).

*4.2 Design of the IMSMC Controller*

The technique proposed in this section is a modification of the classical nonlinear technique, whereby fuzzy logic is used to improve the response and overcome the shortcomings of the classical technique. FL was used because of its advantages such as robustness [60]. Fuzzy logic is among the techniques of artificial intelligence that have been very popular in the field of control, as there are no mathematical rules that limit its use [61]. Fuzzy logic depends on the user experience and the rules of logic. The disadvantage is that the system becomes somewhat heavier the more rules of fuzzy logic are used [60].

IMSMC technique is a combination of fuzzy logic and MSMC technique to overcome the chattering phenomenon and increase the robustness of the traditional MSMC technique. IMSMC technique is a modification of the classical MSMC technique, in which fuzzy logic is used in place of the Sat(u) function. Fig. 6 represents the proposed architecture for IMSMC technique. Through this figure, the proposed controller is simple, inexpensive, easy to implement and not related to the mathematical form of the system, which facilitates its use in complex systems such as 7-phase motors.

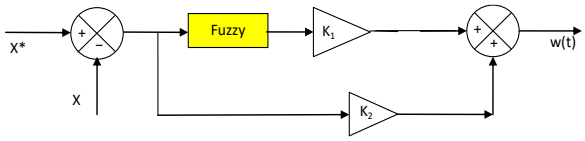


**Fig. 6.** The proposed IMSMC controller

The FL controller used has 2 inputs and one output only, where the two inputs are the error (e) and derivation of error (de/dt). To accomplish this fuzzy logic controller the membership function represented in Fig. 7 [62].

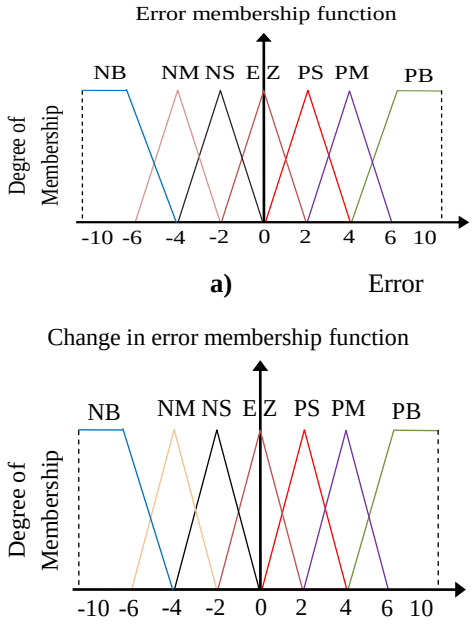


**b)** Change in error

**Fig. 7.** Membership functions.

To accomplish a fuzzy logic controller, fuzzy rules are used. These fuzzy rules are represented in Table 2 [62]. Seven functions are used in the first entry (e) and 7 functions are used in the second entry (de/dt), making the number of rules 49 (7 x 7). 49 fuzzy rules are used to get a good response and thus reduce the ripples of the *Ps*, *Qs*, and torque of the DFIG.

**Table 2.** Fuzzy rules

| e / Δe | NB | NM | NS | EZ | PS | PM | PB |
|---|---|---|---|---|---|---|---|
| **NS** | NB | NB | NM | NS | EZ | PS | PM |
| **PS** | NM | NS | EZ | PS | PM | PB | PB |
| **NM** | NB | NB | NB | NM | NS | EZ | PS |
| **NB** | NB | NB | NB | NB | NM | NS | EZ |
| **PB** | EZ | PS | PM | PB | PB | PB | PB |
| **EZ** | NB | NM | NS | EZ | PS | PM | PB |
| **PM** | NS | EZ | PS | PM | PB | PB | PB |

## 5. DRAPC Based on IMSMC Technique

Fig. 8 represents the proposed DRAPC strategy in this work, where an IMSMC controller is used to minimize the *Ps* and *Qs* ripples of the DFIG-MRWT system. This proposed strategy is a modification of the traditional strategy, where both the proposed IMSMC and PWM technique are used in place of switching table and HCs. The proposed control has several advantages, including durability, ease, low cost of implementation, and low degree of complexity compared to several strategies such as backstepping control

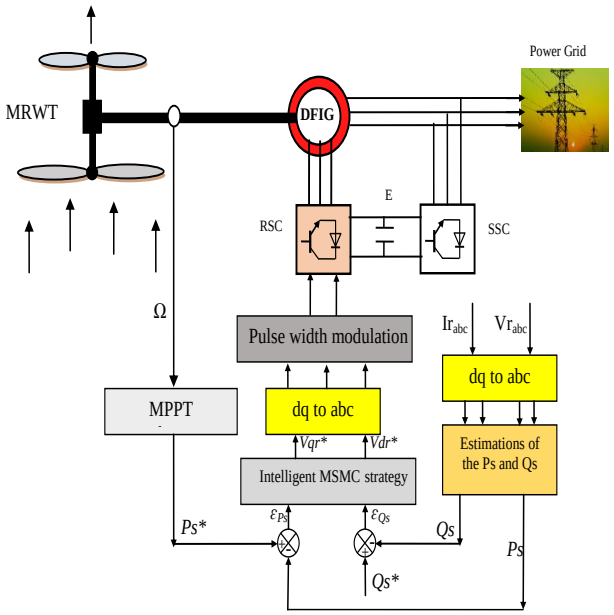


**Fig. 8.** The proposed DRAPC of the DFIG-MRWT system.

In the DRAPC-IMSMC technique, maximum point power tracking (MPPT) is used to find the reference value of the *Ps*. Also, the reference value of the *Qs* is set to 0 VAR.

In this proposed technique, accurate measuring devices are used to measure voltage and current, where these measured values are used to estimate both the *Ps* and *Qs*. In this case,

the same estimation equations used in the classical method are used. In Table 3, the similarities and differences between the two proposed controls in this work are given, as this table was filled using the obtained results. The DRAPC-IMSMC is a control scheme with high characteristics and a higher current quality compared to DRAPC and DRAPC-MSMC techniques.

**Table 3.** A comparative study between the DRAPC-IMSMC and DRAPC-MSMC techniques.

| | **DRAPC-MSMC** | **DRAPC-IMSMC** |
|---|---|---|
| Hysteresis comparator | No | No |
| Simplicity | Simple | Simple |
| Switching table | No | No |
| Steady-state error | High | Low |
| MSVM | Yes | Yes |
| Quality of power | Medium | High |
| Rise time | Medium | Low |
| MSMC controller | Yes | No |
| Robustness | Medium | High |
| MPPT | Yes | Yes |
| *Ps* and *Qs* estimation | Yes | Yes |
| Degree of complexity | Low | Low |
| *Ps* and *Qs* ripples | Medium | Low |
| IMSMC | No | Yes |
| THD | Medium | Low |
| Response dynamic | Quick | Very quick |

## 6. Results

To verify the correctness and behavior of the DRAPC-IMSMC for the DFIG-MRWT system compared to the behavior of the DRAPC-MSMC strategy, Matlab software was used to implement the proposed DRAPC-IMSMC technique and extract the required results. The behavior of the DRAPC-IMSMC was confirmed compared to the DRAPC-MSMC in terms of *Ps* and *Qs* response time, power ripples value, THD of current, and reactive/active power steady-state error. Also, three different tests have been proposed to study the behavior of the DRAPC-IMSMC compared to the DRAPC-MSMC strategy. In addition, a DFIG with a capacity of 1.5 MW was used, as the characteristics of this generator are present in the [53, 41].

### *6.1 First Test*

This test is a reference tracking test to study the behavior of the DRAPC-IMSMC technique. The results obtained are compared with the results of the DRAPC-MSMC. The results are represented in Fig. 9, where the measured active power follows the reference well for the two controls, with a preference for the DRAPC-IMSMC in terms of response time (Fig. 9c). Regarding the measured reactive power, it is not related to the wind speed and takes a constant value equal to 0 VAR (see Fig. 9d).

Fig. 9a represents the current produced by the DFIG-based MRWT system. Comparing Figs 9a and 9c, it can be said that the current is related to the Ps and therefore related to the wind speed. The higher the wind speed, the higher the value of the output current, and in the case of a decrease in the wind speed or a decrease in the value of the active power produced, the value of the current decreases. The same applies to the torque shown in Fig. 9b, where it is noted that the value of torque is related to the value of the measured Ps.

The DRAPC-IMSMC strategy minimized the ripples of torque, *Ps*, current, and *Qs* compared to the DRAPC-MSMC (see Fig. 10). The ripple values are shown in Table 4, where the DRAPC-IMSMC technique minimized ripples by 54.76%, 54.64%, 48%, and 36.50% for the *Qs*, torque, current, and *Ps*, respectively compared to the DRAPC-MSMC. Also, the DRAPC-IMSMC strategy gave excellent results in terms of steady-state error value for both *Ps* and *Qs* (see Table 4). The DRAPC-IMSMC technique reduced the SSE by 54.83% and 54.76% for each of the Ps and Qs, respectively.

The DRAPC-IMSMC strategy provided a good value for THD, which was about 0.49%, and for the DRAPC-MSMC technique, it was about 0.94%. Accordingly, the proposed DRAPC-IMSMC minimized the THD value of the current by an estimated ratio of 47.87% compared to the DRAPC-MSMC strategy.

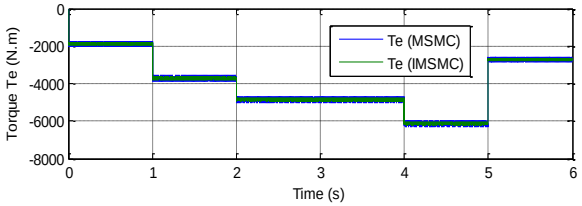


**a)** Current

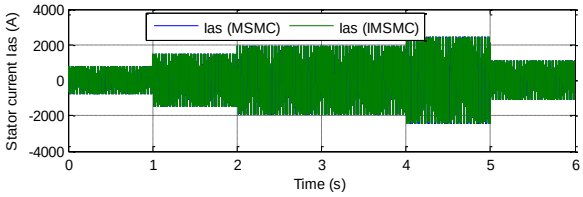


**b)** Torque

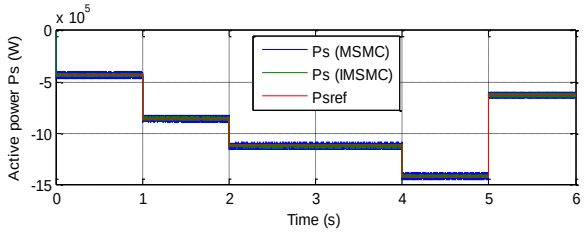


**c)** Active power

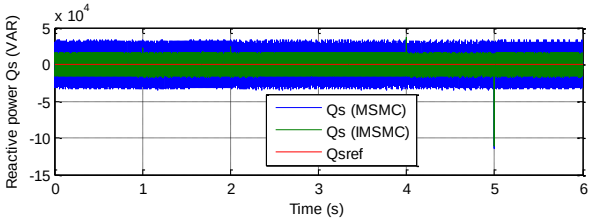

**d)** Reactive power

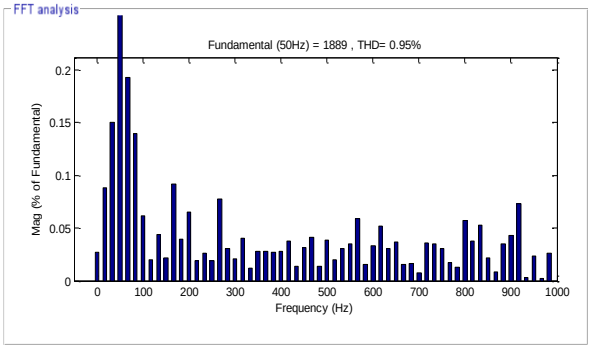


**e)** THD (DRAPC-MSMC)

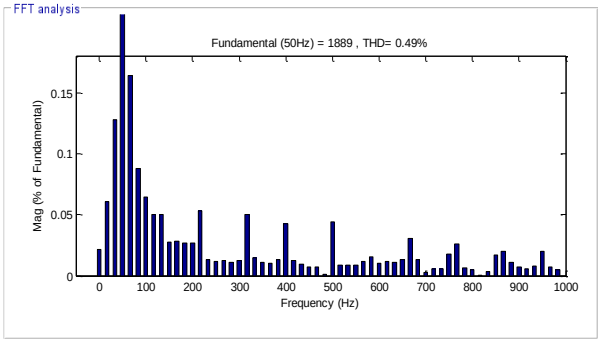


**f)** THD (DRAPC-IMSMC)

**Fig. 9.** First test results

**Table 4.** The SSE value of the *Ps* and *Qs* (First test)

| | Qs (VAR) | Ps (W) |
|---|---|---|
| **DRAPC-MSMC** | 33160 | 31000 |
| **DRAPC-IMSMC** | 15000 | 14000 |
| **Ratios** | 54.76% | 54.83% |

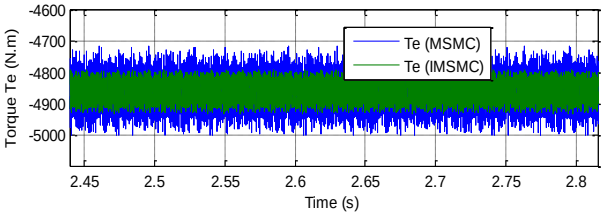


**a)** Torque

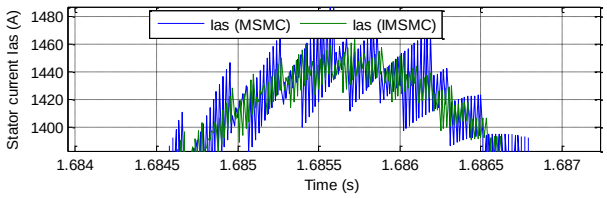


**b)** Torque

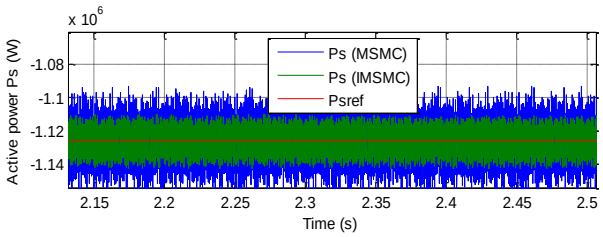


**b)** Active power

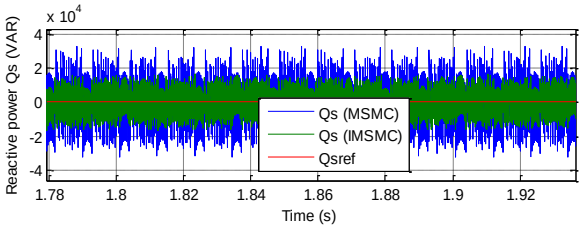


**c)** Reactive power

**Fig. 10.** Zoom in the first test results

**Table 5.** The ripples of the both strategies (First test)

| | Qs (VAR) | Ias (A) | Ps (W) | Te (Nm) |
|---|---|---|---|---|
| **DRAPC-MSMC** | 66320 | 50 | 63000 | 280 |
| **DRAPC-IMSMC** | 30000 | 26 | 40000 | 127 |
| **Ratios** | 54.76% | 48 % | 36.50% | 54.64% |

*6.2 Second Test*

The behavior of the DRAPC-IMSMC in this test is studied in the case of variable wind speed. The obtained results (Fig. 11) are compared with the DRAPC-MSMC technique in terms of power ripple value, THD of current, SSE value and dynamic response. Obtained results are shown in Fig. 11. Through Figs.s 11c and 11d, the measured *Ps* and *Qs* follow the references well for the two strategies, with an advantage for the proposed DRAPC-IMSMC in terms of response time to the *Ps* and *Qs* compared to the DRAPC-MSMC.

The current from the generator is shown in Fig. 11a, where the form of the current is the same as the form of the *Ps*. The value of the current increases with the increase in the value of the *Ps*. The shape of the torque is the same as the shape of the *Ps*, where the value of the torque is affected by the wind speed and increases with the increase in the wind speed (see Fig. 11b).

The designed DRAPC-IMSMC minimized the SSE value for both the *Ps* and the *Qs* compared to the DRAPC-MSMC strategy, where the reduction rates were about 81.48% and 51.51% for each of the *Ps* and *Qs*, respectively (see Table 6).

The current THD value for both techniques is represented in Figs. 11e and 11f. Through these two figures, the proposed DRAPC-IMSMC technique (0.64%) gave a lower value for THD compared to the DRAPC-MSMC (1.25%). Accordingly, the proposed DRAPC-IMSMC minimized the value of the ripples by an estimated 48.80% compared to the DRAPC-MSMC technique.

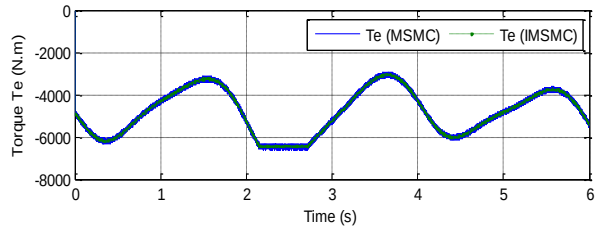


**a)** Torque

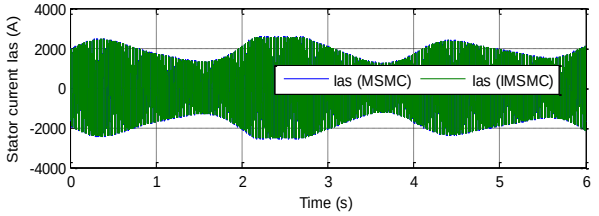


**b)** Current

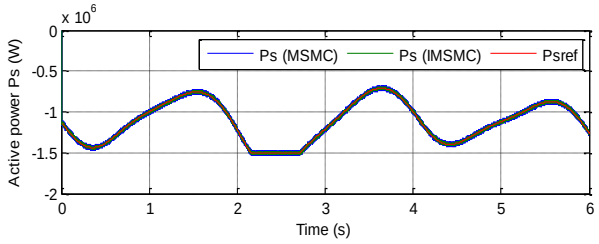


**c)** Active power

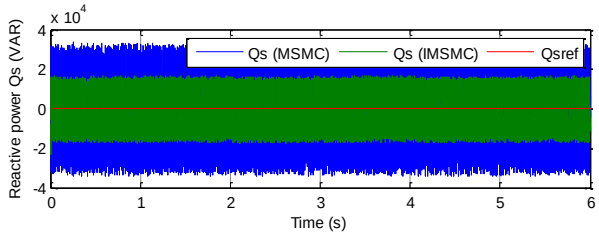


**d)** Reactive power

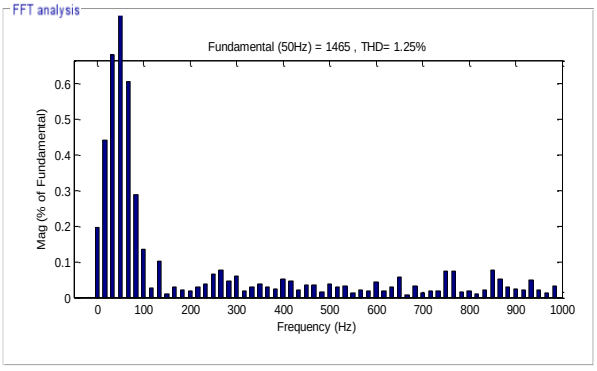


**e)** THD (DRAPC-MSMC)

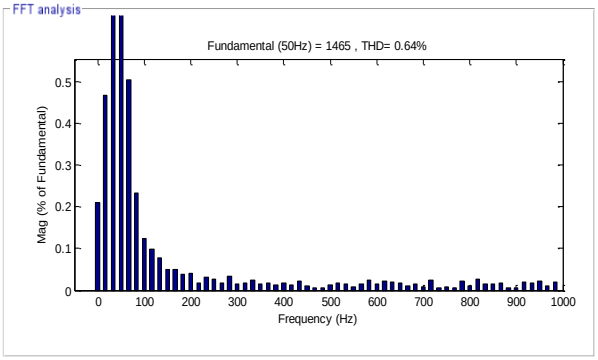


**f)** THD (DRAPC-IMSMC)

**Fig. 11.** Second test results.

**Table 6.** The SSE value of the Qs/Ps (Second test).

| | **Qs (VAR)** | **Ps (W)** |
|---|---|---|
| **DRAPC-MSMC** | 33000 | 27000 |
| **DRAPC-IMSMC** | 16000 | 5000 |
| **Ratios** | 51.51% | 81.48% |

Torque, *Ps*, current, and *Qs* ripples for the two designed DRAPC strategies (see Fig. 12). The proposed DRAPC-IMSMC reduced the value of ripples compared to the classical DRAPC-MSMC strategy for each of the *Ps* and *Qs* compared to the traditional DRAPC-MSMC strategy (see Table 7), where the ratios of reduction were about 95.38%, 44.44%, 51.51%, and 55.55% for each of the *Ps*, current, *Qs* and torque, respectively.

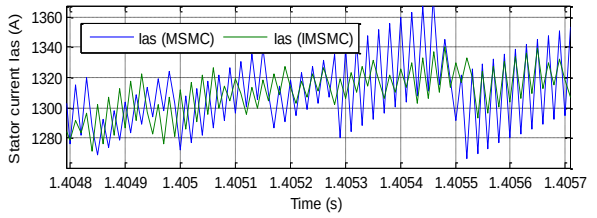


**a)** Current

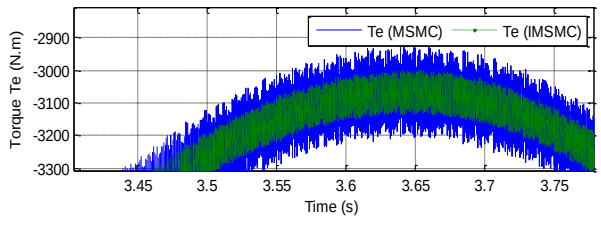


**b)** Torque

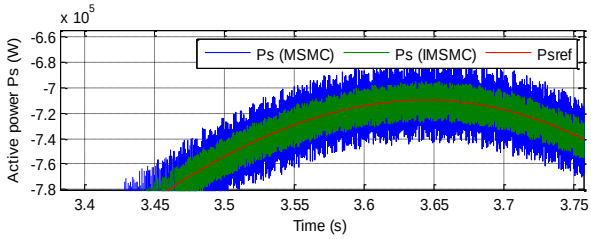


**d)** Active power

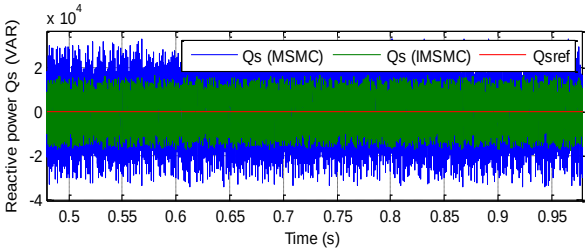


**e)** Reactive power

**Fig. 12.** Zoom in the second test results

**Table 7.** The ripples of the both strategies (Second test)

| | Qs (VAR) | Ias (A) | Ps (W) | Te (Nm) |
|---|---|---|---|---|
| DRAPC-MSMC | 66000 | 45 | 650000 | 270 |
| DRAPC-IMSMC | 32000 | 25 | 30000 | 120 |
| Ratios | 51.51% | 44.44% | 95.38% | 55.55% |

*6.3 Third Test*

In this part, the robustness of the DRAPC-IMSMC is studied, the generator parameters are changed and the behavior of the DRAPC-IMSMC compared to that of the DRAPC-MSMC is studied. The results of this test are shown in Fig. 13. From Fig. 13, the measured *Qs* and *Ps* keep following the references well even thought the generator parameters are changed with ripples (see Figs. 13c and 13d). Also, the DRAPC-IMSMC strategy has the advantage in terms of reducing the value of the SSE and the response time for both the *Qs* and *Ps*. Table 8 represents the SSE values for each of the *Qs* and *Ps*, where the DRAPC-IMSMC technique minimized the value of the SSE by about 45% and 50% ratios for each of the *Ps* and *Qs*.

Regarding current and torque, their values are related to wind speed despite changing the generator parameters (see Figs 13a and 13b). The form of current and torque is the same as for the *Ps*. Fig. 14 represents the ripples of the *Ps*, torque, *Qs* and current for each of the proposed and the DRAPC-MSMC strategy. The ripple values are shown in Table 9. Through this table, the DRAPC-IMSMC was not affected much by changing the DFIG parameters and gave much less ripples than the DRAPC-MSMC technique. Also, the proposed DRAPC-IMSMC technique minimized ripples by 50%, 50%, 42.85%, and 45% ratios compared to the DRAPC-MSMC technique for *Ps*, torque, current, and *Qs*, respectively. The THD of the current was 1.91% for the DRAPC-MSMC technique and 0.88% for the DRAPC-IMSMC. Through these values, the DRAPC-IMSMC minimized the current ripples and improved the current quality, and the reduction ratio was a THD value of 53.92% compared to the DRAPC-MSMC. Through these results, it can be said that the proposed DRAPC-IMSMC is much better than the DRAPC-MSMC strategy in many aspects as a result of using the designed IMSMC controller.

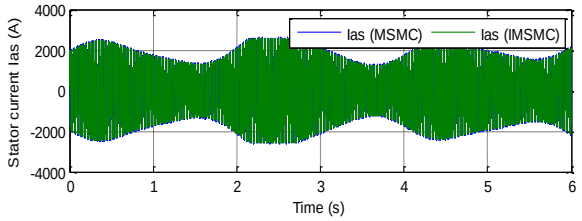


**a)** Current

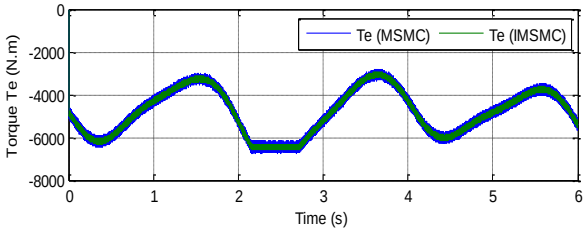


**b)** Torque

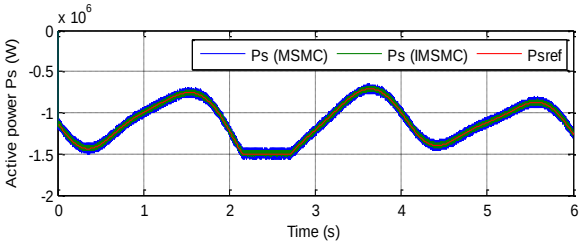


**c)** Active power

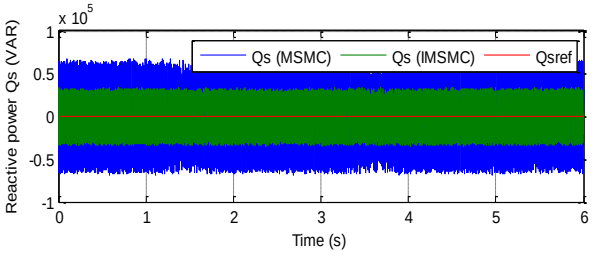


**d)** Reactive power

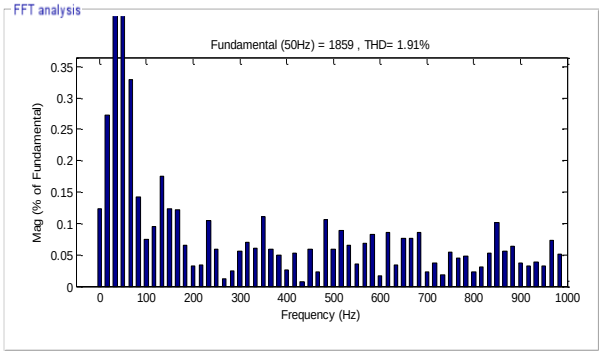


**e)** THD (DRAPC-MSMC)

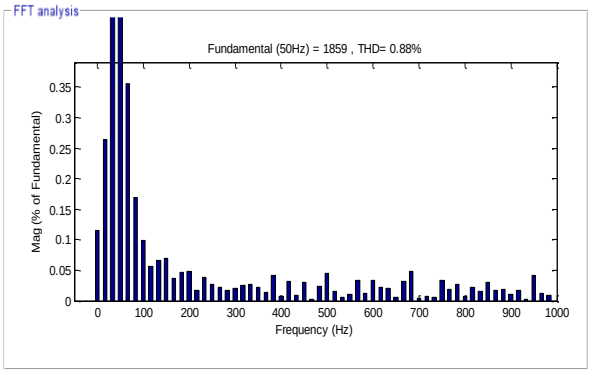


**f)** THD (DRAPC-IMSMC)

**Fig. 13.** Third test results

**Table 8.** The SSE value of the *Ps* and *Qs* (Third test)

| | Ps (W) | Qs (VAR) |
|---|---|---|
| **DRAPC-MSMC** | 60000 | 60000 |
| **DRAPC-IMSMC** | 30000 | 33000 |
| **Ratios** | 50% | 45% |

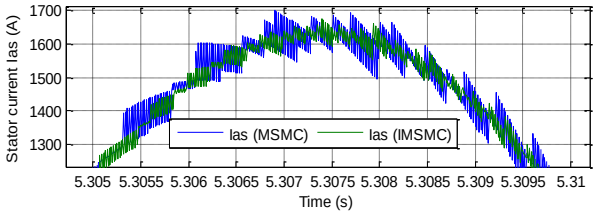


**a)** Current

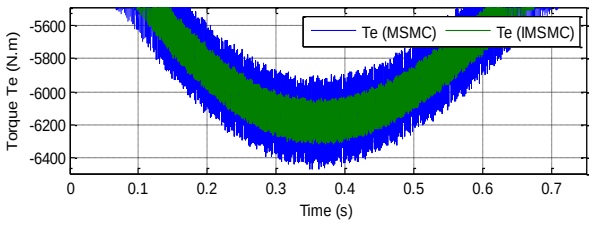


**b)** Torque

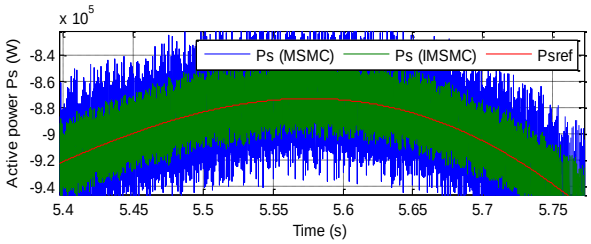


**b)** Active power

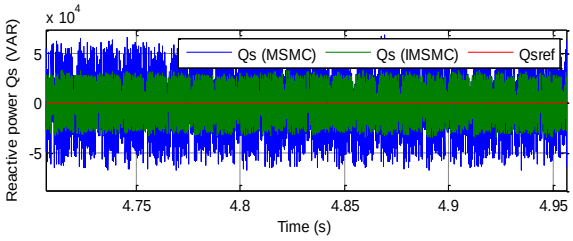


**c)** Reactive power

**Fig. 14.** Zoom in the third test results

**Table 9.** The ripples of the both strategies (Third test)

| | Qs (VAR) | Ias (A) | Ps (W) | Te (Nm) |
|---|---|---|---|---|
| **DRAPC-MSMC** | 120000 | 140 | 120000 | 500 |
| **DRAPC IMSMC** | 66000 | 80 | 60000 | 250 |
| **Ratios** | 45% | 42.85% | 50% | 50% |

## 7. Conclusion

This work presents the simulation results of the DRAPC strategy based on IMSMC controllers of the DFIG-MRWT system, where the obtained results are compared to DRAPC based on MSMC controllers. With results obtained from the simulation, it is clear that for the same operation condition, the DRAPC-IMSMC strategy had good and good characteristics than the DRAPC-MSMC strategy using the modified SVM technique and that is clear in the THD of the current which the use of the proposed IMSMC technique, it is minimized of the harmonic more and more than the MSMC technique.

## References

**1.** T. Surinkaew and I. Ngamroo, " Coordinated Robust Control of DFIG Wind Turbine and PSS for Stabilization of Power Oscillations Considering System Uncertainties, " in IEEE Transactions on Sustainable Energy, Vol. 5, No. 3, pp. 823-833, July 2014, doi: 10.1109/TSTE.2014.2308358.

**2.** I. Alkalbani and F. M. Guangul, " Economical Evaluation of Energy Harvesting Using Vertical Axis Wind Turbine from a Wind Turbulence Created by Moving Cars, " 2021 International Conference on Smart City and Green Energy (ICSCGE), pp. 26-29, 2021, doi: 10.1109/ICSCGE53744.2021.9654414.

**3.** J. R. de Oliveira and A. L. Andreoli, " Wind Turbine Emulator: A Tool for Experimental and Computational

Study, " in IEEE Latin America Transactions, Vol. 19, No. 11, pp. 1832-1839, Nov. 2021, doi: 10.1109/TLA.2021.9475616.

**4.** L. Jia, J. Ma, P. Cheng and Y. Liu, " A perspective on solar energy-powered road and rail transportation in China, " in CSEE Journal of Power and Energy Systems, Vol. 6, No. 4, pp. 760-771, Dec. 2020, doi: 10.17775/CSEEJPES.2020.02040.

**5.** A. S. Al-Sumaiti, A. K. Banhidarah, J. L. Wescoat, A. K. Bamigbade and H. t. Nguyen, " Data Collection Surveys on the Cornerstones of the Water-Energy Nexus: A Systematic Overview, " in IEEE Access, Vol. 8, pp. 93011-93027, 2020, doi: 10.1109/ACCESS.2020.2995054.

**6.** E. A. Bekirov, S. N. Voskresenskaya, M. M. Asanov and E. R. Murtazaev, " Analysis of the Sea Waves Energy Characteristics in the Black Sea Region, " 2020 International Multi-Conference on Industrial Engineering and Modern Technologies (FarEastCon), pp. 1-4, 2020, doi: 10.1109/FarEastCon50210.2020.9271464.

**7.** J. E. Sierra-García and M. Santos, " Improving Wind Turbine Pitch Control by Effective Wind Neuro-Estimators, " in IEEE Access, Vol. 9, pp. 10413-10425, 2021, doi: 10.1109/ACCESS.2021.3051063.

**8.** Z. -C. Zou, X. -Y. Xiao, Y. -F. Liu, Y. Zhang and Y. -H. Wang, " Integrated Protection of DFIG-Based Wind Turbine With a Resistive-Type SFCL Under Symmetrical and Asymmetrical Faults, " in IEEE Transactions on Applied Superconductivity, Vol. 26, No. 7, pp. 1-5, Oct. 2016, Art no. 5603005, doi: 10.1109/TASC.2016.2574352.

**9.** Y. Cui, P. Song, X. S. Wang, W. X. Yang, H. Liu and H. M. Liu, " Wind Power Virtual Synchronous Generator Frequency Regulation Characteristics Field Test and Analysis, " 2018 2nd International Conference on Green Energy and Applications (ICGEA), pp. 193-196, 2018, doi: 10.1109/ICGEA.2018.8356309.

**10.** J. Y. Jin, M. S. Virk, Q. Hu and X. Jiang, " Study of Ice Accretion on Horizontal Axis Wind Turbine Blade Using 2D and 3D Numerical Approach, " in IEEE Access, Vol. 8, pp. 166236-166245, 2020, doi: 10.1109/ACCESS.2020.3022458.

**11.** J. Xie, X. Zhang, S. Huang, F. Huang, Z. Peng, Y. Dai, X. Wu, "Characteristics Simulation Method of Megawatt Three-Blade Horizontal Axis Wind Turbine Based on Laboratory Kilowatt Low-Power Motor System", in IEEE Transactions on Industry Applications, Vol. 58, No. 1, pp. 645-655, Jan.-Feb. 2022, doi: 10.1109/TIA.2021.3123116.

**12.** C. J. Li, R. Bhalla and H. Ling, " Investigation of the Dynamic Radar Signatures of a Vertical-Axis Wind Turbine, " in IEEE Antennas and Wireless Propagation Letters, Vol. 14, pp. 763-766, 2015, doi: 10.1109/LAWP.2014.2377693.

**13.** A. Molina-García, A. Fernández-Guillamón, E. Gómez-Lázaro, A. Honrubia-Escribano and M. C. Bueso, " Vertical Wind Profile Characterization and Identification of Patterns Based on a Shape Clustering Algorithm, " in IEEE Access, Vol. 7, pp. 30890-30904, 2019, doi: 10.1109/ACCESS.2019.2902242.

**14.** O. Beik and A. S. Al-Adsani, " Active and Passive Control of a Dual Rotor Wind Turbine Generator for DC Grids, " in IEEE Access, Vol. 9, pp. 1987-1995, 2021, doi: 10.1109/ACCESS.2020.3047267.

**15.** I. Sami, S. Ullah, L. Khan, A. Al-Durra, J. -S. Ro, " Integer and Fractional-Order Sliding Mode Control Schemes in Wind Energy Conversion Systems: Comprehensive Review, Comparison, and Technical Insight, " Fractal Fract., Vol. 6, 447, 2022. https://doi.org/10.3390/fractalfract6080447.

**16.** L. H. Zheng, X. Q. Li and J. X. Jin, " Characteristic Analysis of High Temperature Superconducting Wind Turbine Generator, " 2020 IEEE International Conference on Applied Superconductivity and Electromagnetic Devices (ASEMD), pp. 1-2, 2020, doi: 10.1109/ASEMD49065.2020.9276203.

**17.** S. Sharma and B. Singh, " Asynchronous Generator With Battery Storage for Standalone Wind Energy Conversion System, " in IEEE Transactions on Industry Applications, Vol. 50, No. 4, pp. 2760-2767, July-Aug. 2014, doi: 10.1109/TIA.2013.2295475.

**18.** K. Shi, W. Song, H. Ge, P. Xu, Y. Yang and F. Blaabjerg, " Transient Analysis of Microgrids With Parallel Synchronous Generators and Virtual Synchronous Generators, " in IEEE Transactions on Energy Conversion, Vol. 35, No. 1, pp. 95-105, March 2020, doi: 10.1109/TEC.2019.2943888.

**19.** D. H. Wang, C. V. Nayar and C. Wang, " Modeling of stand-alone variable speed diesel generator using doubly-fed induction generator, " The 2nd International Symposium on Power Electronics for Distributed Generation Systems, pp. 1-6, 2010, doi: 10.1109/PEDG.2010.5545769.

**20.** T. Suzuki, H. Okitsu, T. Kawahito, " Characteristics of a small wind-power system with DC generator, " IEE Proc. - Electr. Power Appl., Vol. 129, pp. 217-220, 1982.

**21.** Y. Bakou, M. Abid, A. Harrouz, I. Yaichi, I. Colak, K. Kayisli, A. Aissaoui, " DTC Control of the DFIG, Application to the Production of Electrical Energy, " 2019 8th International Conference on Renewable Energy Research and Applications (ICRERA), pp. 910-915, 2019, doi : 10.1109/ICRERA47325.2019.8996947.

**22.** M. El Azzaoui, H. Mahmoudi and C. Ed-dahmani, " Backstepping control of a Doubly Fed Induction Generator integrated to wind power system, " 2016 International Conference on Electrical and Information Technologies (ICEIT), pp. 306-311, 2016, doi : 10.1109/EITech.2016.7519611.

**23.** H. Benbouhenni, " Synergetic control theory scheme for asynchronous generator based dual-rotor wind power, " Journal of Electrical Engineering, Electronics, Control and Computer Science, Vol.7, No.3, pp.19-28, 2021.

**24.** H. Benbouhenni, "A comparison study between fuzzy PWM and SVM inverter in NSMC control of stator active and reactive power control of a DFIG based wind turbine systems, " International Journal of Applied Power Engineering (IJAPE), Vol. 8, No. 1, pp. 78-92, 2019.

**25.** H. Benbouhenni, Z. Boudjema, A. Belaidi, "DPC based on ANFIS super-twisting sliding mode algorithm of a doubly-fed induction generator for wind energy system, " Journal Européen des Systèmes Automatisés, Vol. 53, No. 1, pp. 69-80, February, 2020.

**26.** J. Mohammadi, S. Vaez-Zadeh, S. Afsharnia and E. Daryabeigi, " A Combined Vector and Direct Power Control for DFIG-Based Wind Turbines, " in IEEE Transactions on

Sustainable Energy, Vol. 5, No. 3, pp. 767-775, July 2014, doi : 10.1109/TSTE.2014.2301675.

**27.** S. Salem, A. Rabeh, A. Nesrine, C. Souad, " Passivity-Based Direct power control of Shunt Active Filter under Distorted Grid Voltage Conditions, " Automatika, 2016, Vol. 57, No. 2, pp. 361-371, 2016. DOI : 10.7305/automatika.2016.10.1011.

**28.** M. Valikhani and C. Sourkounis, " Improvements on robustness of hysteresis-based vector control of DFIG using brain emotional leaning-based intelligent controller (BELBIC), " 2014 Ninth International Conference on Ecological Vehicles and Renewable Energies (EVER), pp. 1-5, 2014, doi: 10.1109/EVER.2014.6844084.

**29.** J. Erazo-Damián, J. M. Apsley, R. Perini, M. F. Iacchetti and G. D. Marques, " Stand-Alone DFIG FOC Sensitivity and Stability Under Mismatched Inductances, " in IEEE Transactions on Energy Conversion, Vol. 34, No. 2, pp. 860-869, June 2019, doi: 10.1109/TEC.2018.2869286.

**30.** J. Hu, H. Nian, B. Hu, Y. He and Z. Q. Zhu, " Direct Active and Reactive Power Regulation of DFIG Using Sliding-Mode Control Approach, " in IEEE Transactions on Energy Conversion, Vol. 25, No. 4, pp. 1028-1039, Dec. 2010, doi: 10.1109/TEC.2010.2048754.

**31.** B. Hu, H. Nian, J. Yang, M. Li and Y. Xu, " High-Frequency Resonance Analysis and Reshaping Control Strategy of DFIG System Based on DPC, " in IEEE Transactions on Power Electronics, Vol. 36, No. 7, pp. 7810-7819, July 2021, doi: 10.1109/TPEL.2020.3045860.

**32.** R. M. Prasad and M. A. Mulla, " Rotor Position-Sensorless Algorithms for Direct Power Control of Rotor-Tied DFIG, " in IEEE Transactions on Power Electronics, Vol. 36, No. 6, pp. 6213-6217, June 2021, doi: 10.1109/TPEL.2020.3040705.

**33.** X. Wang, D. Sun and Z. Q. Zhu, " Resonant-Based Backstepping Direct Power Control Strategy for DFIG Under Both Balanced and Unbalanced Grid Conditions, " in IEEE Transactions on Industry Applications, Vol. 53, No. 5, pp. 4821-4830, Sept.-Oct. 2017, doi: 10.1109/TIA.2017.2700280.

**34.** Y. Zhang, J. Jiao, D. Xu, " Direct Power Control of Doubly Fed Induction Generator Using Extended Power Theory Under Unbalanced Network, " in IEEE Transactions on Power Electronics, Vol. 34, No. 12, pp. 12024-12037, 2019. doi: 10.1109/TPEL.2019.2906013.

**35.** Z. Zhang, F. Wang, J. Wang, J. Rodríguez and R. Kennel, " Nonlinear Direct Control for Three-Level NPC Back-to-Back Converter PMSG Wind Turbine Systems: Experimental Assessment With FPGA, " in IEEE Transactions on Industrial Informatics, Vol. 13, No. 3, pp. 1172-1183, June 2017, doi: 10.1109/TII.2017.2678500.

**36.** H. Kong, J. He, Y. Liu, P. Cheng and J. Ma, " Improved Direct Power Control of Doubly Fed Induction Generator Without Phase-Locked Loop, " 2020 IEEE Sustainable Power and Energy Conference (iSPEC), pp. 199-204, 2020, doi: 10.1109/iSPEC50848.2020.9351036.

**37.** H. Benbouhenni, " Two-level DPC strategy based on FNN algorithm of the DFIG-DRWT systems using two-level hysteresis controllers for reactive and active powers, " Renewable Energy Research and Application (RERA), Vol.2, No.3, pp.137-146, 2021, http://dx.doi.org/10.22044/rera.2021.10694.1053.

**38.** M. Pichan, H. Rastegar and M. Monfared, " Fuzzy-based direct power control of doubly fed induction generator-based wind energy conversion systems, " 2012 2nd International Conference on Computer and Knowledge Engineering (ICCKE), pp. 66-70, 2012, doi: 10.1109/ICCKE.2012.6395354.

**39.** H. Benbouhenni, " Application of DPC and DPC-GA to the dual-rotor wind turbine system with DFIG, " International Journal of Robotics and Automation, Vol.10, No.3, pp. 224-234, 2021, Doi: 10.11591/ijra.v10i3.pp224-234.

**40.** P. Xiong and D. Sun, " Backstepping-Based DPC Strategy of a Wind Turbine-Driven DFIG Under Normal and Harmonic Grid Voltage, " in IEEE Transactions on Power Electronics, vol. 31, no. 6, pp. 4216-4225, June 2016, doi: 10.1109/TPEL.2015.2477442.

**41.** H. Benbouhenni, N. Bizon, "Terminal Synergetic Control for direct active and reactive powers in Asynchronous Generator-based Dual-Rotor Wind Power Systems," Electronics, Vol.10, No.16, pp.1-23, 2021. https://doi.org/10.3390/electronics10161880.

**42.** A. Susperregui, M. I. Martínez, G. Tapia-Otaegui and A. Etxeberria, " Sliding-Mode Control Algorithm for DFIG Synchronization to Unbalanced and Harmonically Distorted Grids, " in IEEE Transactions on Sustainable Energy, Vol. 13, No. 3, pp. 1566-1579, July 2022, doi: 10.1109/TSTE.2022.3166217.

**43.** S. S. Yu, G. Zhang, T. Fernando and H. H. -C. Iu, " A DSE-Based SMC Method of Sensorless DFIG Wind Turbines Connected to Power Grids for Energy Extraction and Power Quality Enhancement, " in IEEE Access, Vol. 6, pp. 76596-76605, 2018, doi: 10.1109/ACCESS.2018.2883591.

**44.** J. Hu, H. Nian, B. Hu, Y. He and Z. Q. Zhu, " Direct Active and Reactive Power Regulation of DFIG Using Sliding-Mode Control Approach, " in IEEE Transactions on Energy Conversion, Vol. 25, No. 4, pp. 1028-1039, Dec. 2010, doi: 10.1109/TEC.2010.2048754.

**45.** D. Sun, X. Wang, H. Nian and Z. Q. Zhu, " A Sliding-Mode Direct Power Control Strategy for DFIG Under Both Balanced and Unbalanced Grid Conditions Using Extended Active Power, " in IEEE Transactions on Power Electronics, Vol. 33, No. 2, pp. 1313-1322, Feb. 2018, doi: 10.1109/TPEL.2017.2686980.

**46.** L. Shang and J. Hu, " Sliding-Mode-Based Direct Power Control of Grid-Connected Wind-Turbine-Driven Doubly Fed Induction Generators Under Unbalanced Grid Voltage Conditions, " in IEEE Transactions on Energy Conversion, Vol. 27, No. 2, pp. 362-373, June 2012, doi: 10.1109/TEC.2011.2180389.

**47.** I. Sami, S. Ullah, S. U. Amin, A. Al-Durra, N. Ullah and J. -S. Ro, " Convergence Enhancement of Super-Twisting Sliding Mode Control Using Artificial Neural Network for DFIG-Based Wind Energy Conversion Systems, " in IEEE Access, Vol. 10, pp. 97625-97641, 2022, doi: 10.1109/ACCESS.2022.3205632.

**48.** R. Galindo del Valle, M. Cotorogea Pfeifer and D. Biel Sole, " Two families of sliding mode controllers for a doubly-fed induction generator in an isolated generation system, " in IEEE Latin America Transactions, vol. 5, no. 2, pp. 115-121, May 2007, doi: 10.1109/TLA.2007.4381353.

**49.** N. Nasiri and N. Yousefi Lademakhi, " Nonlinear combined SMC-SDRE control versus SMC and SDRE approaches for electrical flexible-joint robots based on optimal observer, " 2021 9th RSI International Conference on Robotics and Mechatronics (ICRoM), pp. 568-573, 2021, doi: 10.1109/ICRoM54204.2021.9663514.

**50.** A. Wahyu Aditya, M. Rizani Rusli, B. Praharsena, E. Purwanto, D. Cahya Happyanto and B. Sumantri, " The Performance of FOSMC and Boundary - SMC in Speed Controller and Current Regulator for IFOC-Based Induction Motor Drive, " 2018 International Seminar on Application for Technology of Information and Communication, pp. 139-144, 2018, doi: 10.1109/ISEMANTIC.2018.8549842.

**51.** L. Shang and J. Hu, " Sliding-Mode-Based Direct Power Control of Grid-Connected Wind-Turbine-Driven Doubly Fed Induction Generators Under Unbalanced Grid Voltage Conditions, " in IEEE Transactions on Energy Conversion, Vol. 27, No. 2, pp. 362-373, June 2012, doi: 10.1109/TEC.2011.2180389.

**52.** H. Benbouhenni, " Sliding mode with neural network regulateur for DFIG using two-level NPWM strategy, " Iranian Journal of Electrical & Electronic Engineering, Vol. 15, No. 3, pp.411-419, 2019.

**53.** H. Benbouhenni, Z. Boudjema, N. Bizon, P. Thounthong, N. Takorabet, " Direct Power Control Based on Modified Sliding Mode Controller for a Variable-Speed Multi-Rotor Wind Turbine System Using PWM Strategy, " Energies, Vol. 15, No. 10, 2022. https://doi.org/10.3390/en15103689.

**54.** W. Yang, A. Zhang, J. Li, G. Li, H. Zhang, J. Wang, " Integral Plus Resonant Sliding Mode Direct Power Control for VSC-HVDC Systems under Unbalanced Grid Voltage Conditions, " Energies, Vol. 10, 1528, 2017. https://doi.org/10.3390/en10101528.

**55.** M. Farida, S. Belkacem and I. Colak, " Fuzzy High Order Sliding Mode Control Based DPC of DFIG using SVM, " 2021 9th International Conference on Smart Grid (icSmartGrid), pp. 278-282, 2021, doi: 10.1109/icSmartGrid52357.2021.9551262.

**56.** H. Benbouhenni, N. Bizon, I. Colak, P. Thounthong, N. Takorabet, " Application of Fractional-Order PI Controllers and Neuro-Fuzzy PWM Technique to Multi-Rotor Wind Turbine Systems, " Electronics 2022, 11, 1340. https://doi.org/10.3390/electronics11091340.

**57.** H. Benbouhenni, N. Bizon, " Advanced Direct Vector Control Method for Optimizing the Operation of a Double-Powered Induction Generator-Based Dual-Rotor Wind Turbine System, " Mathematics, Vol.9, No.19, 2297, 2021, doi: 10.3390/math9182297.

**58.** H. Benbouhenni, N. Bizon, " Third-Order Sliding Mode Applied to the Direct Field-Oriented Control of the Asynchronous Generator for Variable-Speed Contra-Rotating Wind Turbine Generation Systems, " Energies, Vol. 14, No.18, 1-17, 2021. https://doi.org/10.3390/en14185877

**59.** H. Benbouhenni, N. Bizon, " Improved Rotor Flux and Torque Control Based on the Third-Order Sliding Mode Scheme Applied to the Asynchronous Generator for the Single-Rotor Wind Turbine, " Mathematics, Vol. 9, No.18, 2297. https://doi.org/10.3390/math9182297.

**60.** J. M. Mendel and D. Wu, " Critique of A New Look at Type-2 Fuzzy Sets and Type-2 Fuzzy Logic Systems, " in IEEE Transactions on Fuzzy Systems, vol. 25, no. 3, pp. 725-727, June 2017, doi: 10.1109/TFUZZ.2017.2648882.

**61.** L. -X. Wang, " A New Look at Type-2 Fuzzy Sets and Type-2 Fuzzy Logic Systems, " in IEEE Transactions on Fuzzy Systems, Vol. 25, No. 3, pp. 693-706, June 2017, doi: 10.1109/TFUZZ.2016.2543746.

**62.** H. Benbouhenni, " Five-level DTC control of induction machine drive using fuzzy logic controller for low torque ripple," Acta Technica Corviniensis-Bulletin of Engineering, Vol. 12, No. 2, pp. 91-96, 2019.